

The Measurement of AM noise of Oscillators

Enrico Rubiola

web page <http://rubiola.org>



FEMTO-ST Institute
CNRS and Université de Franche Comté, Besançon, France

9th December 2005

Abstract

The close-in AM noise is often neglected, under the assumption that it is a minor problem as compared to phase noise. With the progress of technology and of experimental science, this assumption is no longer true. Yet, information in the literature is scarce or absent.

This report describes the measurement of the AM noise of rf/microwave sources in terms of $S_\alpha(f)$, i.e., the power spectrum density of the fractional amplitude fluctuation α . The proposed schemes make use of commercial power detectors based on Schottky and tunnel diodes, in single-channel and correlation configuration.

There follow the analysis of the front-end amplifier at the detector output, the analysis of the methods for the measurement of the power-detector noise, and a digression about the calibration procedures.

The measurement methods are extended to the relative intensity noise (RIN) of optical beams, and to the AM noise of the rf/microwave modulation in photonic systems.

Some rf/microwave synthesizers and oscillators have been measured, using correlation and moderate averaging. As an example, the flicker noise of a low-noise quartz oscillator (Wenzel 501-04623E) is $S_\alpha = 1.15 \times 10^{-13} / f$, which is equivalent to an Allan deviation of $\sigma_\alpha = 4 \times 10^{-7}$. The measurement systems described exhibit the world-record lowest background noise.

Symbol list

$\bar{\cdot}$, as in $\bar{v}(t)$	average, or dc component [of the signal $v(t)$]
$\tilde{\cdot}$, as in $\tilde{v}(t)$	ac component [of the signal $v(t)$]
B	system bandwidth
$\mathbb{E}\{\cdot\}$	statistical expectation
f	Fourier frequency (near dc)
g	voltage gain (thus, the power gain is g^2)
h	$h = 6.626 \times 10^{-34}$ J/Hz, Planck constant
h_i	coefficient of the power-law representation of noise, $S(f) = \sum_i h_i f^i$
$i(t), I$	current, dc current
$I(t), I_0$	optical intensity (Sections 9–10)
k	1.38×10^{-23} J/K, Boltzmann constant
k_d	detector gain, V/W. Also k_a, k_b, k_c
m	in cross-spectrum measurements, no. of averaged spectra
m	modulation index (Sections 9–10)
P, P_0	carrier power. Also P_a, P_b, P_m , etc.
q	$q = 1.602 \times 10^{-19}$ C, electron charge
R	resistance
R_0	characteristic resistance. Often $R_0 = 50 \Omega$
rms	root mean square value
$S(f), S_x(f)$	single-sided power spectrum density (of the quantity x)
t	time
T, T_0	absolute temperature, reference temperature ($T_0 = 290$ K)
$v(t)$	(voltage) signal, as a function of time
V_0	peak carrier voltage (not accounting for noise)
V_T	$V_T = \frac{kT}{q}$ thermal voltage. $V_T \approx 25.6$ mV at 25 °C
$\alpha(t)$	fractional amplitude fluctuation
δ , as in δx	random fluctuation (of the quantity x)
Δ , as in Δx	deterministic fluctuation (of the quantity x)
η	diode technical parameter [Eq.(15)], $\eta \in [1..2]$
η	photodetector quantum efficiency (Sections 9–10)
λ	wavelength
λ , as in ν_λ	in a subscript, λ means ‘light’ (as opposed to ‘microwave’)
μ , as in ν_μ	in a subscript, μ means ‘microwave’ (as opposed to ‘light’)
ν, ν_0	frequency, carrier frequency
ϱ	photodetector responsivity, A/W (Sections 9–10)
$\sigma_x(\tau)$	Allan deviation of the quantity x
τ , as in $\sigma_x(\tau)$	measurement time
$\varphi(t)$	phase fluctuation

Contents

Symbol list	2
1 Basics	4
2 Single channel measurement	5
3 Dual channel (correlation) measurement	7
4 Schottky and tunnel diode power detectors	8
5 The double balanced mixer	12
6 Power detector noise	13
7 Design of the front-end amplifier	15
8 The measurement of the power detector noise	23
9 AM noise in optical systems	23
10 AM noise in microwave photonic systems	27
11 Calibration	29
12 Examples	32
13 Final remarks	37
References	37

1 Basics

A quasi-perfect rf/microwave sinusoidal signal can be written as

$$v(t) = V_0 [1 + \alpha(t)] \cos[2\pi\nu_0 t + \varphi(t)] , \quad (1)$$

where $\alpha(t)$ is the fractional amplitude fluctuation, and $\varphi(t)$ is the phase fluctuation. Equation (1) defines $\alpha(t)$ and $\varphi(t)$. In low noise conditions, that is, $|\alpha(t)| \ll 1$ and $|\varphi(t)| \ll 1$, Eq. (1) is equivalent to

$$\begin{aligned} v(t) &= V_0 \cos(2\pi\nu_0 t) + v_c(t) \cos(2\pi\nu_0 t) - v_s(t) \sin(2\pi\nu_0 t) \\ \text{with } \alpha(t) &= \frac{1}{V_0} v_c(t) \quad \text{and} \quad \varphi(t) = \frac{1}{V_0} v_s(t) . \end{aligned} \quad (2)$$

We make the following assumptions about $v(t)$, in agreement with actual cases of interest:

1. The expectation of the amplitude is V_0 . Thus $\mathbb{E}\{\alpha(t)\} = 0$.
2. The expectation of the frequency is ν_0 . Thus $\mathbb{E}\{\dot{\varphi}(t)\} = 0$.
3. Low noise. $|\alpha(t)| \ll 1$ and $|\varphi(t)| \ll 1$.
4. Narrow band. The bandwidth of α and φ is $B_\alpha \ll \nu_0$ and $B_\varphi \ll \nu_0$.

It is often convenient to describe the close-in noise in terms of the single-side¹ power spectrum density $S(f)$, as a function of the Fourier frequency f . A model that has been found useful to describe $S(f)$ is the power-law $S(f) = \sum_i h_i f^i$. In the case of amplitude noise, generally the spectrum contains only the white noise $h_0 f^0$, the flicker noise $h_{-1} f^{-1}$, and the random walk $h_{-2} f^{-2}$. Accordingly,

$$S_\alpha(f) = h_0 + h_{-1} f^{-1} + h_{-2} f^{-2} . \quad (3)$$

Random walk and higher-slope phenomena, like drift, are often induced by the environment. It is up to the experimentalist to judge the effect of environment.

The spectrum density can be converted into Allan variance using the formulae of Table 2.

The signal power is

$$P = \frac{V_0^2}{2R} (1 + \alpha)^2 \quad (4)$$

thus

$$P \simeq \frac{V_0^2}{2R} (1 + 2\alpha) \quad \text{because } \alpha \ll 1 \quad (5)$$

¹Most experimentalists prefer the single-side power spectrum density because all instruments work in this way. This is because the power can be calculated as $P = \int_0^B S(f) df$, which is far more straightforward than integrating over positive and (to some extent, mysterious) negative frequencies.

Table 2: Relationships between power spectrum density and Allan variance.

noise type	Spectrum density $S_\alpha(f)$	Allan variance $\sigma_\alpha^2(\tau)$
white	h_0	$\frac{h_0}{2\tau}$
flicker	$h_{-1}f^{-1}$	$h_{-1} 2 \ln(2)$
random walk	$h_{-2}f^{-2}$	$h_{-2} \frac{4\pi^2}{6} \tau$

It is convenient to rewrite P as $P = P_0 + \delta P$, with

$$P_0 = \frac{V_0^2}{2R} \quad \text{and} \quad \delta P \simeq 2P_0\alpha \quad (6)$$

The amplitude fluctuations are measured through the measurement of the power fluctuation δP ,

$$\alpha(t) = \frac{1}{2} \frac{\delta P}{P_0} \quad (7)$$

and of its power spectrum density,

$$S_\alpha(f) = \frac{1}{4} S_{\frac{\delta P}{P_0}}(f) = \frac{1}{4P_0^2} S_P(f) . \quad (8)$$

The measurement of a two-port device, like an amplifier, is made easy by the availability of the reference signal sent to the device input. In this case, the bridge (interferometric) method [RG02] enables the measurement of amplitude noise and phase noise with outstanding sensitivity. Yet, the bridge method can not be exploited for the measurement of the AM noise of oscillators, synthesizers and other signal sources. Other methods are needed, based on power detectors and on suitable signal processing techniques.

2 Single channel measurement

Figure 1 shows the basic scheme for the measurement of AM noise. The detector characteristics (Sec. 4) is $v_d = k_d P$, hence the ac component of the detected signal is $\tilde{v}_d = k_d \delta P$. The detected voltage is related to α by $\tilde{v}_d = k_d P_0 \frac{\delta P}{P_0}$, that is,

$$\tilde{v}_d(t) = 2k_d P_0 \alpha(t) . \quad (9)$$

Turning voltages into spectra, the above becomes

$$S_v(f) = 4k_d^2 P_0^2 S_\alpha(f) . \quad (10)$$

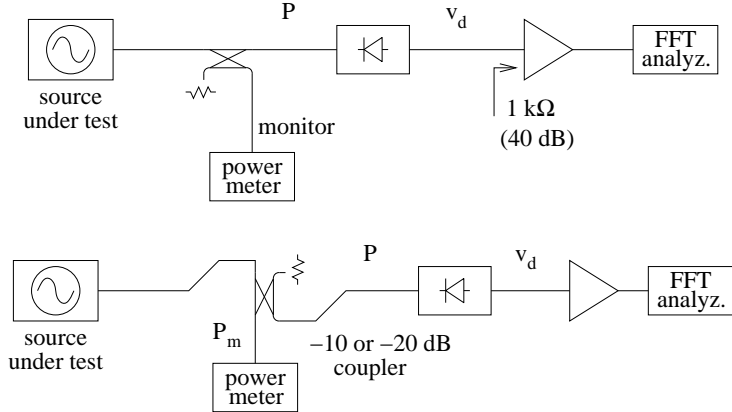


Figure 1: Top: Basic scheme for the measurement of AM noise. Bottom: A variant useful in some cases where the power detector operates at low power, while the power meter does not.

Therefore, the spectrum of α can be measured using

$$S_\alpha(f) = \frac{1}{4k_d^2 P_0^2} S_v(f) . \quad (11)$$

Due to linearity of the network that precedes the detector (directional couplers, cables, etc.), the fractional power fluctuation $\delta P/P_0$ is the same in all the circuit, thus α is the same. As a consequence, the separate measurement of the oscillator power and of the attenuation from the oscillator to the detector is not necessary. The straightforward way to use Eq. (10), or (11), is to refer P_0 at detector input, and v_d at the detector output.

Interestingly, phase noise has virtually no effect on the measurement. This happens because the bandwidth of the detector is much larger than the maximum frequency of the Fourier analysis, hence no memory effect takes place.

In single-channel measurements, the background noise can only be assessed by measuring a low-noise source². Of course, this measurement gives the total noise of the source and of the instrument, which can not be divided. The additional hypothesis is therefore required, that the amplitude noise of the source is lower than the instrument background. Unfortunately, a trusted source will be hardly available in practice.

Calibration is needed, which consists of the measurement of the product $k_d P_0$. See Section 11.

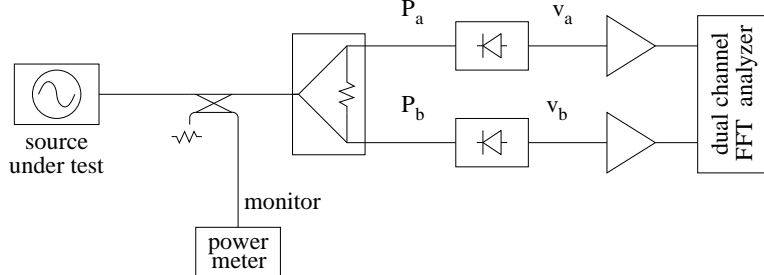


Figure 2: Correlation AM noise measurement.

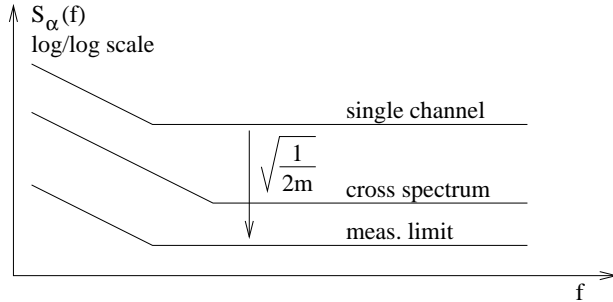


Figure 3: Spectra of the correlation AM noise measurement.

3 Dual channel (correlation) measurement

Figure 2 shows the scheme for the correlation measurement of AM noise. The signal is split into two branches, and measured by two separate power detectors and amplifiers. Under the assumption that the two channels are independent, the cross spectrum $S_{ba}(f)$ is proportional to $S_\alpha(f)$. In fact, the two dc signals are $v_a = k_a P_a \alpha$ and $v_b = k_b P_b \alpha$. The cross spectrum is

$$S_{ba}(f) = 4k_a k_b P_a P_b S_\alpha(f) , \quad (12)$$

from which

$$S_\alpha(f) = \frac{1}{4k_a k_b P_a P_b} S_{ba}(f) . \quad (13)$$

Averaging over m spectra, the noise of the individual channels is rejected by a factor $\sqrt{2m}$ (Fig. 3), for the sensitivity can be significantly increased. A further advantage of the correlation method is that the measurement of $S_\alpha(f)$ is validated by the simultaneous measurement of the instrument noise limit, that is, the single-channel noise divided by $\sqrt{2m}$. This solves one of the major problems of the single-channel measurement, i.e., the need of a trusted low-noise source.

²The reader familiar with phase noise measurements is used to measure the instrument noise by removing the device under test. This is not possible in the case of the AM noise of the oscillator.

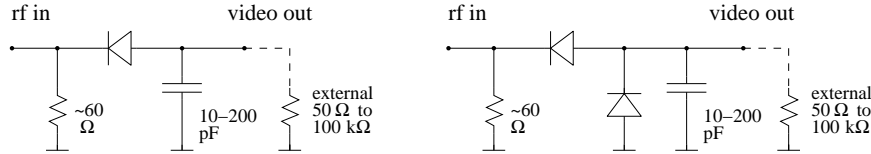


Figure 4: Scheme of the diode power detector.

Larger is the power delivered by the source under test, larger is the instrument gain. This applies to single-channel measurements, where the gain is $4k_d^2 P_0^2$ [Eq. (10)], and to correlation measurements, where the gain is $4k_a k_b P_a P_b$ [Eq. (12)]. Yet in a correlation system the total power P_0 is split into the two channels, for $P_a P_b = \frac{1}{4} P_0^2$. Hence, switching from single-channel to correlation the gain drops by a factor $\frac{1}{4}$ (-6 dB). Let us now compare a correlation system to a single-channel system under the simplified hypothesis that the background noise referred at the detector output is unchanged. This happens if the noise of the dc preamplifier is dominant. In such cases, the background noise referred to the instrument input, thus to S_α , is multiplied by a factor $\frac{4}{\sqrt{2m}}$. The numerator “4” arises from the reduced gain, while the denominator $\sqrt{2m}$ is due to averaging. Accordingly, it must be $m > 8$ for the correlation scheme to be advantageous in terms of sensitivity. On the other hand, if the power of the source under test is large enough for the system to work at full gain in both cases, the dual-channel system exhibits higher sensitivity even at $m = 1$.

Calibration is about the same as for the single-channel measurements. See Section 11.

In laboratory practice, the availability of a dual-channel FFT analyzer is the most frequent critical point. If this instrument is available, the experimentalist will prefer the correlation scheme in virtually all cases.

4 Schottky and tunnel diode power detectors

A rf/microwave power detector uses the nonlinear response of a diode to turn the input power P into a dc voltage v_d . The transfer function is

$$v_d = k_d P , \quad (14)$$

which defines the detector gain k_d . The physical dimension of k_d is A^{-1} . The technical unit often used in data sheets is mV/mW , equivalent to A^{-1} . The diodes can only work at low input level. Beyond a threshold power, the output voltage differs smoothly from Eq. (14). The actual response depends on the diode type.

Figure 4 shows the scheme of actual power detectors. The input resistor matches the high input impedance of the diode network to the standard value $R_0 = 50 \Omega$ over the bandwidth and over the power range. The value depends on

Table 3: some power-detector manufacturers (non-exhaustive list).

manufacturer	web site
Aeroflex/Metelics	aeroflex-metelics.com
Agilent Technologies	agilent.com
Advanced Control Components	advanced-control.com
Advanced Microwave	advancedmicrowaveinc.com
Eclipse	eclipsemicrowave.com
Herotek	herotek.com
Microphase	microphase.com/military/detectors.shtml
Omniyig	omniyig.com
RLC Electronics	rlcelectronics.com/detectors.htm
S-Team	s-team.sk

Table 4: Typical characteristics of Schottky and tunnel power detectors.

	Schottky	tunnel
input bandwidth	up to 4 decades 10 MHz to 20 GHz	1–3 octaves up to 40 GHz
VSVR max.	1.5:1	3.5:1
max. input power (spec.)	–15 dBm	–15 dBm
absolute max. input power	20 dBm or more	20 dBm
output resistance	1–10 kΩ	50–200 Ω
output capacitance	20–200 pF	10–50 pF
gain	300 V/W	1000 V/W
cryogenic temperature	no	yes

the specific detector. The output capacitor filters the video³ signal, eliminating carrier from the output. A low capacitance makes the detector fast. On the other hand, a higher capacitance is needed if the detector is used to demodulate a low-frequency carrier. The two-diode configuration provides larger output voltage and some temperature compensation.

Power detectors are available off-the-shelf from numerous manufacturers, some of which are listed on Table 3. Agilent Technologies provides a series of useful application notes [Agi03] about the measurement of rf/microwave power.

Two types of diode are used in practice, Schottky and tunnel. Their typical characteristics are shown in Table 4.

Schottky detectors are the most common ones. The relatively high output resistance and capacitance makes the detector suitable to low-frequency carriers, starting from some 10 MHz (typical). In this condition the current flowing

³From the early time of electronics, the term ‘video’ is used (as opposed to ‘audio’) to emphasize the large bandwidth of the demodulated signal, regardless of the real purposes.

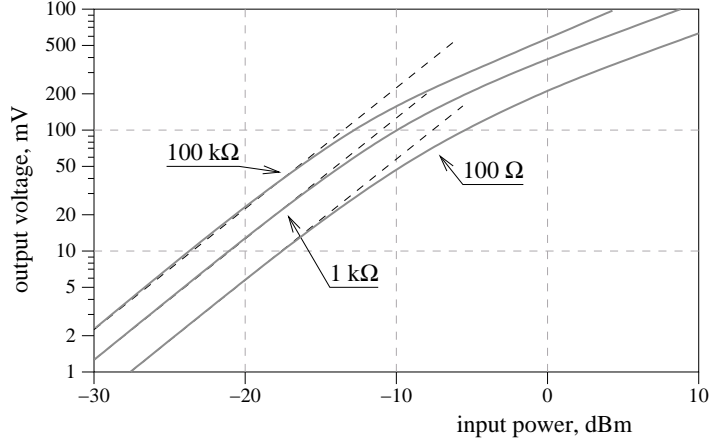


Figure 5: Response of a two-diode power detector.

through the diode is small, and the input matching to $R_0 = 50 \Omega$ is provided by a low value resistor. Thus, the VSWR is close to 1:1 in a wide frequency range. Most of the input power is dissipated in the input resistance, which reduces the risk of damage in case of overload. A strong preference for negative output voltage seems to derive from the lower noise of P type Schottky diodes, as compared to N type ones, in conjunction with practical issues of mechanical layout. Figure 5 shows the response of a two-diode Schottky power detector. The quadratic response [Eq. (14)] derives from the diode resistance R_d , which is related to the saturation current I_0 by

$$R_d = \frac{\eta V_T}{q I_0} , \quad (15)$$

where $\eta \in [1 \dots 2]$ is a parameter that derives from the junction technology; $V_T = kT/q \simeq 25.6$ mV at room temperature is the thermal voltage. At higher input level, R_d becomes too small and the detector response turns smoothly from quadratic to linear, like the response of the common AM demodulators and power rectifiers.

Tunnel detectors are actually *backward* detectors. The backward diode is a tunnel diode in which the negative resistance in the forward-bias region is made negligible by appropriate doping, and used in the reverse-bias region. Most of the work on such detectors dates back to the sixties [Bur63, Gab67, Hal60]. Tunnel detectors exhibit fast switching and higher gain than the Schottky counterpart. A low output resistance is necessary, which affects the input impedance. Input impedance matching is therefore poor. In the measurement of AM noise, as in other applications in which fast response is not relevant, the output resistance can be higher than the recommended value, and limited only by noise considerations. At higher output resistance the gain further increases. Tunnel diodes also work in cryogenic environment, provided the package tolerates the mechanical stress of the thermal contraction.

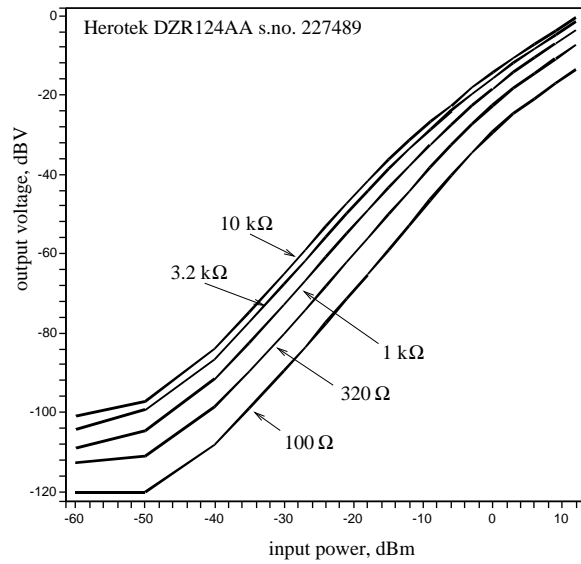


Figure 6: Measured response of a Schottky detector Herotek DZR124AA.

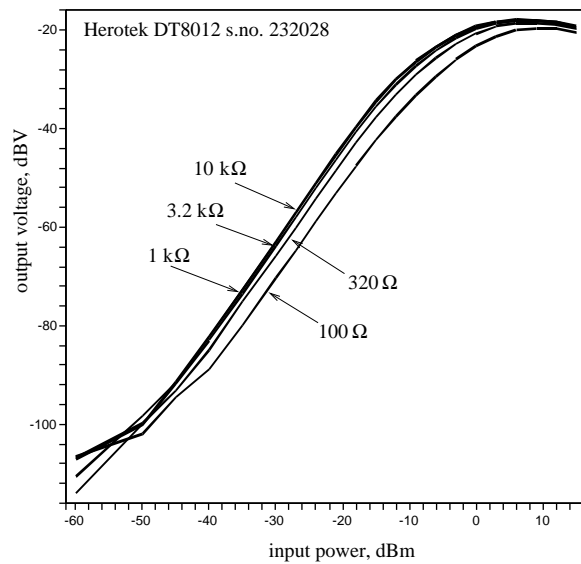


Figure 7: Measured response of a tunnel detector Herotek DT8012.

Table 5: Measured conversion gain.

load resistance, Ω	detector gain, A^{-1}	
	DZR124AA (Schottky)	DT8012 (tunnel)
1×10^2	35	292
3.2×10^2	98	505
1×10^3	217	652
3.2×10^3	374	724
1×10^4	494	750
conditions: power -50 to -20 dBm		

Figures 6–7 and Table 5 show the conversion gain of two detectors, measured at the FEMTO-ST Institute. As expected, the Schottky detector leaves smoothly the quadratic law (true power detection) at some -12 dBm, where it becomes a peak voltage detector. The response of the tunnel detector is quadratic up to a maximum power lower than that of the Schottky diode. This is due to the lower threshold of the tunnel effect. The output voltage shows a maximum at some 0 dBm, then decreases. This is ascribed to the tunnel-diode conduction in the forward region.

At the FEMTO-ST Institute, I routinely use the Herotek DZR124AA (Schottky) and DT8012 (tunnel). At the JPL, I have sometimes used the pair HP432A, and more recently the same Herotek types that I use at the LPMO. The old HP432A pair available shows an asymmetry of almost 10 dB in flickering, which causes experimental difficulties. This asymmetry might be a defect of the specific sample.

5 The double balanced mixer

Some articles from the NIST [NNW94]⁴ suggest the use of a double balanced mixer as the power detector in AM noise measurements, with a configuration similar to that of Fig. 8. Higher sensitivity is obtained with cross-spectrum measurements, using two mixers. The double balanced mixer is operated in the following conditions:

1. Both RF and LO inputs are *not* saturated.
2. The RF and LO signals are in-phase.

At low frequencies the in-phase condition may be hard wired, omitting the variable phase shifter.

⁴Fred Walls published some articles in the FCS Proceedings. Craig Nelson showed the method in his tutorial given at the 2003 FCS.

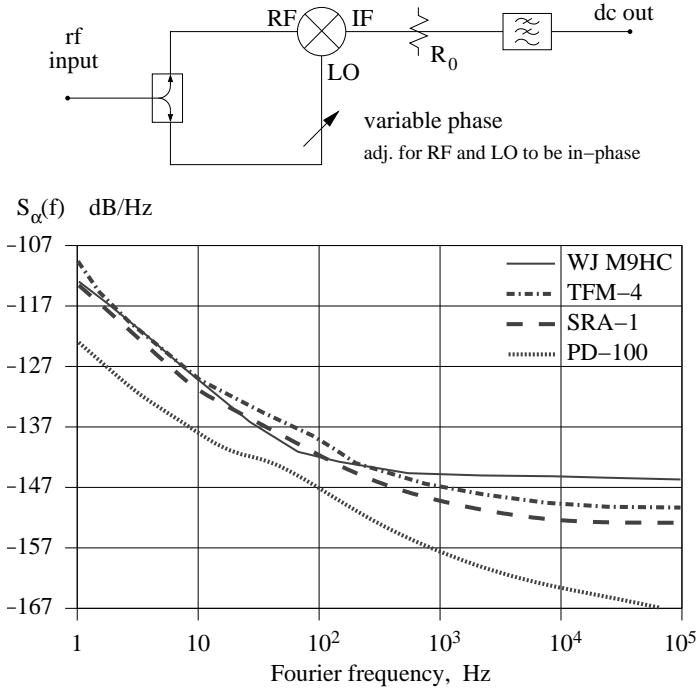


Figure 8: A double balanced mixer can be used as the power detector for the measurement of AM noise. Data are from [NNW94].

However useful, the available articles do not explain the diode operation in terms of electrical parameters. One can expect that the background noise of the mixer used as the AM detector can not be lower than that of a Schottky-diode power detector for the simple reason that the mixer contains a ring of Schottky diodes. One could guess that the use of the mixer for AM noise measurements originates from having had mixers and phase shifter on hand for a long time at the NIST department of phase noise.

6 Power detector noise

Two fundamental types of noise are present in a power detector, shot noise and thermal noise [Gab67, Sec. V]. In addition, detectors show flicker noise. The latter is not explained theoretically, for the detector characterization relies on experimental parameters. Some useful pieces of information are available in [Eng61].

Owing to the shot effect, the average current \bar{i} flowing in the diode junction is affected by a fluctuation of power spectral density

$$S_i = 2q\bar{i} \quad \text{A}^2/\text{Hz}, \quad (16)$$

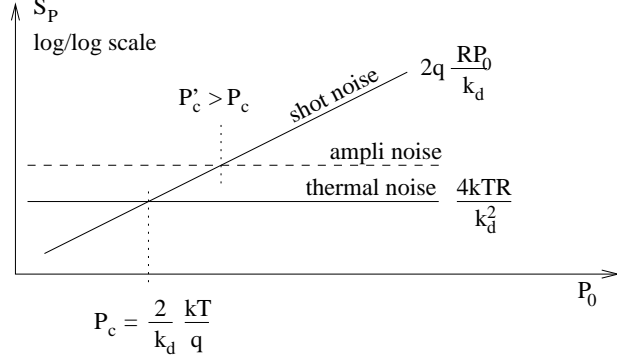


Figure 9: Power spectral density of the detector noise, referred at the input.

Using the Ohm law $v = Ri$ across the load resistor R , the noise voltage at the detector output is

$$S_v = 2qR\bar{v} \quad \text{V}^2/\text{Hz}. \quad (17)$$

Then, the shot noise is referred to the input-power noise using $v = k_dP$. Thus, at the operating power P_0 it holds that

$$S_P = 2q \frac{RP_0}{k_d} \quad \text{shot noise, W}^2/\text{Hz}. \quad (18)$$

The thermal noise across load resistance R has the power spectral density

$$S_v = 4kTR \quad \text{V}^2/\text{Hz}, \quad (19)$$

which turns into

$$S_P = \frac{4kTR}{k_d^2} \quad \text{thermal noise, W}^2/\text{Hz}. \quad (20)$$

referred to the detector input. An additional thermal-noise contribution comes from the dissipative resistance of the diodes. This can be accounted for by increasing the value of R in Equations (19) and (20). It should be remarked that diode differential resistance is not a dissipative phenomenon, for there is no thermal noise associated to it.

Figure 9 shows the equivalent input noise as a function of power. The shot noise is equal to the thermal noise, $(S_P)_{\text{shot}} = (S_P)_{\text{thermal}}$, at the critical power

$$P_c = \frac{2}{k_d} \frac{kT}{q}. \quad (21)$$

It turns out that the power detector is always used in the low power region ($P_0 < P_c$), where shot noise is negligible. In fact, taking the data of Table 5 as typical of actual detectors, P_c spans from +2 dBm to -10 dBm for the Schottky

diodes ($35 \text{ A}^{-1} < k_d < 500 \text{ A}^{-1}$), and from -8 dBm to -12 dBm for the tunnel diodes ($330 \text{ A}^{-1} < k_d < 820 \text{ A}^{-1}$), depending on the load resistance. On the other hand, the detector turns from the quadratic (power) response to the linear (voltage) response at a significantly lower power. This can be seen on Figure 6 and 7.

Looking at the specifications of commercial power detectors, information about noise is scarce. Some manufacturers give the NEP (Noise Equivalent Power) parameter, i.e., the power at the detector input that produces a video output equal to that of the device noise. In no case is said whether the NEP increases or not in the presence of a strong input signal, which is related to precision. Even worse, no data about flickering is found in the literature or in the data sheets. Only one manufacturer (Herotek) claims the low flicker feature of its tunnel diodes, yet without providing any data.

The power detector is always connected to some kind of amplifier, which is noisy. Denoting with $(h_0)_{\text{ampli}}$ and $(h_{-1})_{\text{ampli}}$ the white and flicker noise coefficients of the amplifier, the spectrum density referred at the input is

$$S_P(f) = \frac{(h_0)_{\text{ampli}}}{k_d^2} + \frac{(h_{-1})_{\text{ampli}}}{k_d^d} \frac{1}{f}. \quad (22)$$

The amplifier noise coefficient $(h_0)_{\text{ampli}}$ is connected to the noise figure by $(h_0)_{\text{ampli}} = (F - 1)kT$. Yet we prefer not to use the noise figure because in general the amplifier noise results from voltage noise and current noise, which depends on R . Equation (22) is rewritten in terms of amplitude noise using $\alpha = \frac{1}{2} \frac{\delta P}{P_0}$ [Eq. (7)]. Thus,

$$S_\alpha(f) = \frac{1}{2P_0} \frac{qR}{k_d} + \frac{1}{P_0^2} \frac{kTR}{k_d^2} + \frac{1}{4P_0^2} \frac{(h_0)_{\text{ampli}}}{k_d^2} + \frac{1}{4P_0^2} \frac{(h_{-1})_{\text{ampli}}}{k_d^2} \frac{1}{f}. \quad (23)$$

After the first term of Eq. (22), the critical power becomes

$$P'_c = \frac{2}{k_d} \frac{kT}{q} + \frac{(h_0)_{\text{ampli}}}{2qRk_d}. \quad (24)$$

This reinforces the conclusion that in actual conditions the shot noise is negligible.

7 Design of the front-end amplifier

For optimum design, one should account for the detector noise and for the noise of the amplifier, and find the most appropriate amplifier and operating conditions. Yet, the optimum design relies upon the detailed knowledge of the power-detector noise, which is one of our targets (Sec. 8). Thus, we provisionally neglect the excess noise of the power detector. The first design is based on the available data, i.e., thermal noise and the noise of the amplifier. Operational amplifiers or other types of impedance-mismatched amplifiers are often used in practice. As a consequence, a single parameter, i.e., the noise figure or the

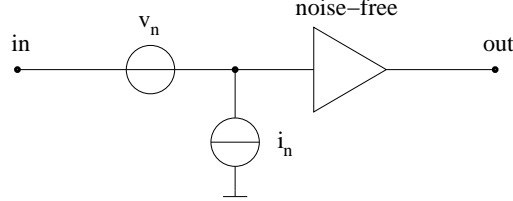


Figure 10: Rothe-Dahlke model of the noisy amplifier.

noise temperature, is not sufficient to describe the amplifier noise. Voltage and current fluctuations must be treated separately, according to the popular Rothe-Dahlke model [RD56] (Fig. 10). The amplifier noise contains white and flicker, thus

$$(S_v)_{\text{ampli}} = h_{0,v} + h_{-1,v} \frac{1}{f} \quad (25)$$

$$(S_i)_{\text{ampli}} = h_{0,i} + h_{-1,i} \frac{1}{f} . \quad (26)$$

The design can be corrected afterwards, accounting for the flicker noise of the detector.

Single-channel systems

Accounting for shot and thermal noise, and for the noise of the amplifier, the noise spectrum density is

$$S_v = 2qR\bar{v} + 4kTR + (S_v)_{\text{ampli}} + R^2 (S_i)_{\text{ampli}} \quad (27)$$

at the amplifier input, and

$$S_P = 2q \frac{RP}{k_d} + \frac{4kTR}{k_d^2} + \frac{(S_v)_{\text{ampli}}}{k_d^2} + \frac{R^2 (S_i)_{\text{ampli}}}{k_d^2} \quad (28)$$

referred to the rf input. The detector gain k_d depends on R , thus the residual S_P can not be arbitrarily reduced by decreasing R . Instead, there is an optimum R at which the system noise is at its minimum.

Correlation-and-averaging systems

The noise contribution of the amplifier can be reduced by measuring the cross spectrum at the output of two amplifiers connected to the power detector, provided that the noise of the amplifiers is independent. For this to be true, the optimum design of the front-end amplifier changes radically. Figure 11 points out the problem. The current noise of each amplifier turns into a random voltage fluctuation across the load resistance R . Focusing only on the amplifier

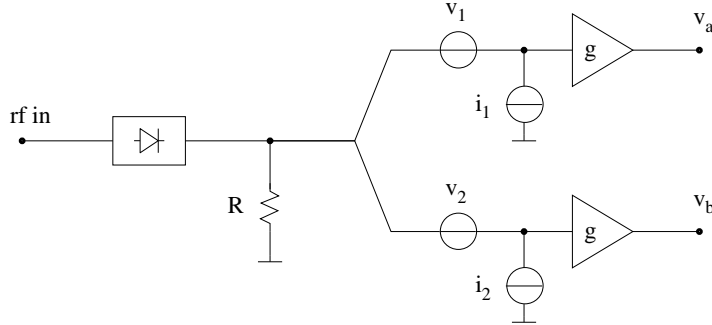


Figure 11: The load resistor turns the current noise into fully-correlated noise.

noise, the voltage at the two outputs is

$$\begin{aligned} v_a &= g(v_1 + Ri_1 + Ri_2) \\ v_b &= g(v_2 + Ri_1 + Ri_2) \end{aligned}$$

The terms gv_1 and gv_2 are independent, for their contribution to the cross spectrum density is reduced by a factor $\frac{1}{\sqrt{2m}}$, where m is the number of averaged spectra. Conversely, a term

$$gR(i_1 + i_2)$$

is present at the two outputs. This term is exactly the same, thus it can not be reduced by correlation and averaging. Consequently, the lowest current noise is the most important parameter, even if this is obtained at expense of a larger voltage noise. Yet, the rejection of larger voltage noise requires large m , for some tradeoff may be necessary.

Examples

This section shows some design attempts, aimed at the lowest white and flicker noise at low Fourier frequencies, up to 0.1–1 MHz, where operational amplifiers can be exploited in a simple way.

A preliminary analysis reveals that, at the low resistance values required by the detector, BJT amplifiers perform lower noise than field-effect transistors. On the other hand, the noise rejection by correlation and average requires low current noise, for JFET amplifiers are the best choice. In fact, BJTs can not be used because of the current noise, while MOSFETs show $1/f$ noise significantly larger (10 dB or more) than JFETs.

Using two detectors (DZR124AA and DT8012), we try the operational amplifiers and transistor pairs listed on Table 6. These amplifiers are selected with the criterion that each one is a low-noise choice in its category.

AD743 and OPA627 are general-purpose precision JFET amplifiers, which exhibit low bias current, hence low current noise. They are intended for

Table 6: Noise parameters of some selected amplifiers.

type	voltage		current		notes
	white $h_{0,v}$	flicker $h_{-1,v}$	white $h_{0,i}$	flicker $h_{-1,i}$	
AD743	2.9	18	6.9	—	jfet op-amp
LT1028	0.9	1.7	1000	16	bjt op-amp
MAT02	0.9	1.6	900	1.6	npn bjt matched pair
MAT03	0.7	1.2	1200	11	pnp bjt matched pair
OP27	3.0	4.3	400	4.7	bjt op-amp
OP177	10	8.0	125	1.6	bjt op-amp
OP1177	8.0	8.3	200	1.5	bjt op-amp
OPA627	4.5	45	2.5	—	jfet op-amp
unit	$\frac{\text{nV}}{\sqrt{\text{Hz}}}$	$\frac{\text{nV}}{\sqrt{\text{Hz}}}$	$\frac{\text{fA}}{\sqrt{\text{Hz}}}$	$\frac{\text{pA}}{\sqrt{\text{Hz}}}$	

correlation-and-averaging schemes (Fig. 11). The **OP625** is similar to the OP627 but for the frequency compensation, which enables unity-gain operations, yet at expenses of speed. It is used successfully in the measurement of the excess noise of semiconductors, where large averaging size is necessary in order to rid of the amplifier noise [SFF99].

LT1028 is a fast BJT amplifier with high bias current in the differential input stage. This feature makes it suitable to low-noise applications in which the source resistance is low. In fact, the optimum noise resistance $R_b = \sqrt{h_v/h_i}$ is of $900\ \Omega$ for white noise, and of $105\ \Omega$ for flicker. These values are in the preferred range for proper operation of the power detectors.

MAT02 and **MAT03** are bipolar matched pairs. They exhibit lower noise than operational amplifiers, and they are suitable to the design for low resistance of the source, like the LT1028. The MAT03 was successfully employed in the design of a low-noise amplifier optimized for $50\ \Omega$ sources [RLV04].

OP27 and **OP37** are popular general-purpose precision BJT amplifiers, most often used in low-noise applications. Their noise characteristics are about identical. The OP27 is fully compensated, for it is stable at closed-loop gain of one. The OP37 is only partially compensated, which requires a minimum closed-loop gain of five for stable operation. Of course, lower compensation increases bandwidth and speed.

OP177 and **OP1177** are general-purpose precision BJT amplifiers with low bias current in the differential input stage, thus they exhibit lower current noise than other BJT amplifiers. They can be an alternative if the design based on JFET amplifier fails.

In the try-and-error process, we take into account shot noise, thermal noise, amplifier voltage noise, and amplifier current noise. The total white noise is the sum of all them

$$S_P = 2q \frac{RP}{k_d^2} + \frac{4kTR}{k_d^2} + \frac{h_{0,v}}{k_d^2} + \frac{R^2 h_{0,i}}{k_d^2} \quad \text{total white [+] .} \quad (29)$$

The total flicker accounts for the voltage and current of the amplifier

$$S_P = \frac{h_{-1,v}}{k_d^2} + \frac{R^2 h_{-1,i}}{k_d^2} \quad \text{total flicker [\diamond] .} \quad (30)$$

The correlated noise spectrum is equal to the total noise minus the voltage noise spectrum of the amplifier, which is independent

$$S_P = 2q \frac{RP}{k_d^2} + \frac{4kTR}{k_d^2} + \frac{R^2 h_{0,i}}{k_d^2} \quad \text{correlated white [\circ] ,} \quad (31)$$

$$S_P = \frac{R^2 h_{-1,i}}{k_d^2} \quad \text{correlated flicker [\square] .} \quad (32)$$

The flicker noise of the detector, still not available, is to be added to Equations (30) and (32).

After evaluation, we discard the OP177 because the OP1177 exhibits superior performances in all noise parameters. Similarly, we discard the OP627 in favour of the AD743. The lower current noise of the OP627 can be exploited only at very large number of averages, which is impractical. On the other hand, the lower voltage noise of the AD743 helps to keep the number of averages reasonable. Figures 12 and 13 show a summary of the expected noise as a function of the load resistance R . The symbols $+$, \circ , \diamond , \square have the same meaning in Equations (29)–(32) and in Figures 12 and 13. Analyzing the noise plots we restrict our attention to the detector-amplifier pairs of Table 7, in which we identify the following interesting configurations.

Detector DZR124AA (Schottky)

AD743 and 3.2 kΩ. Best design for a correlation-and-averaging system. In principle, lower white noise can be achieved with lower load resistance, yet only with $m > 10^4$.

MAT02 and 1 kΩ. Lowest flicker in real-time measurements (single-channel).

OP27 and 1 kΩ. Simple nearly-optimum design if one is interested to white noise. In fact, the white noise is 1.5 dB higher than that of the two above configurations; this gap increases only at $m > 300$ if the AD743 (jfet) is used. On the other hand, the flicker noise is high and can not be reduced by correlation.

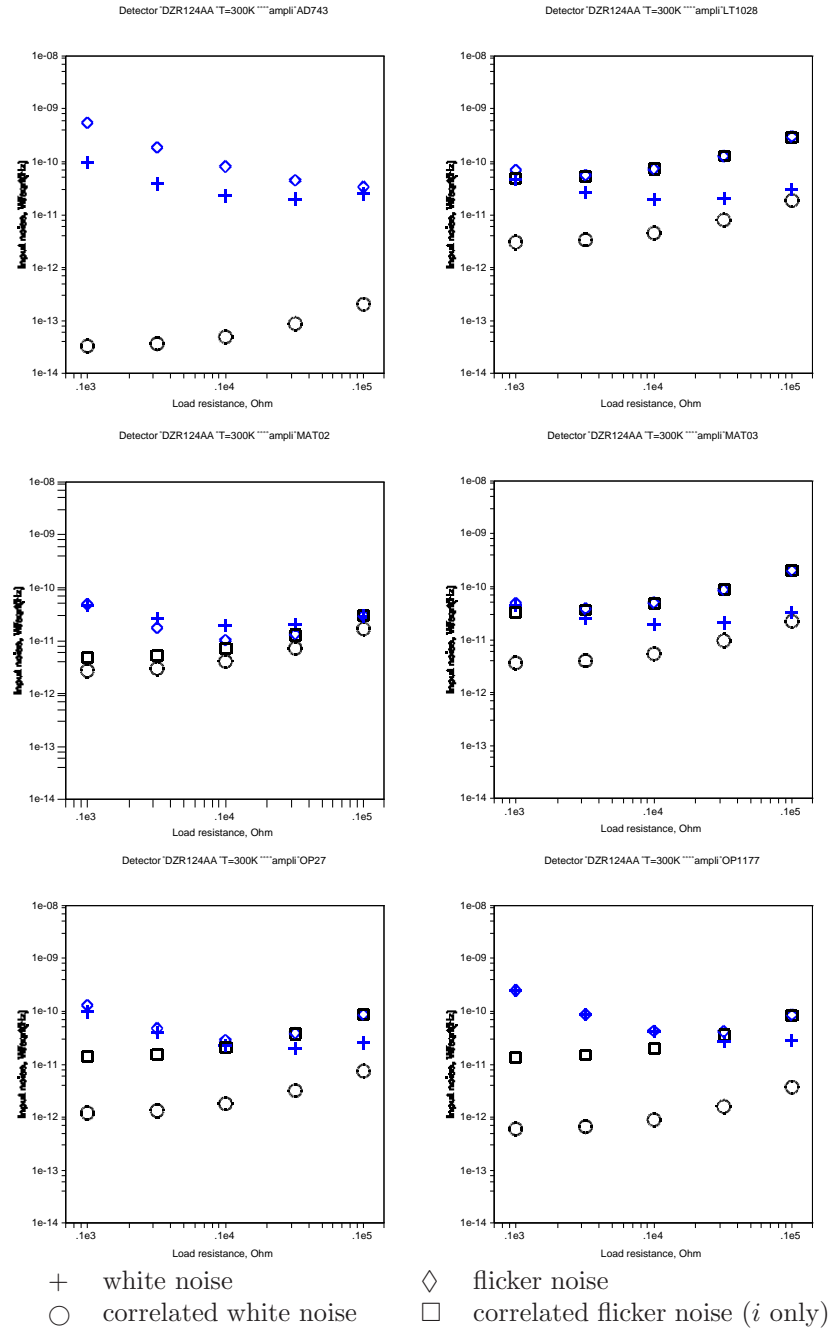


Figure 12: Expected noise of the DZR124AA (Schottky) followed an amplifier.

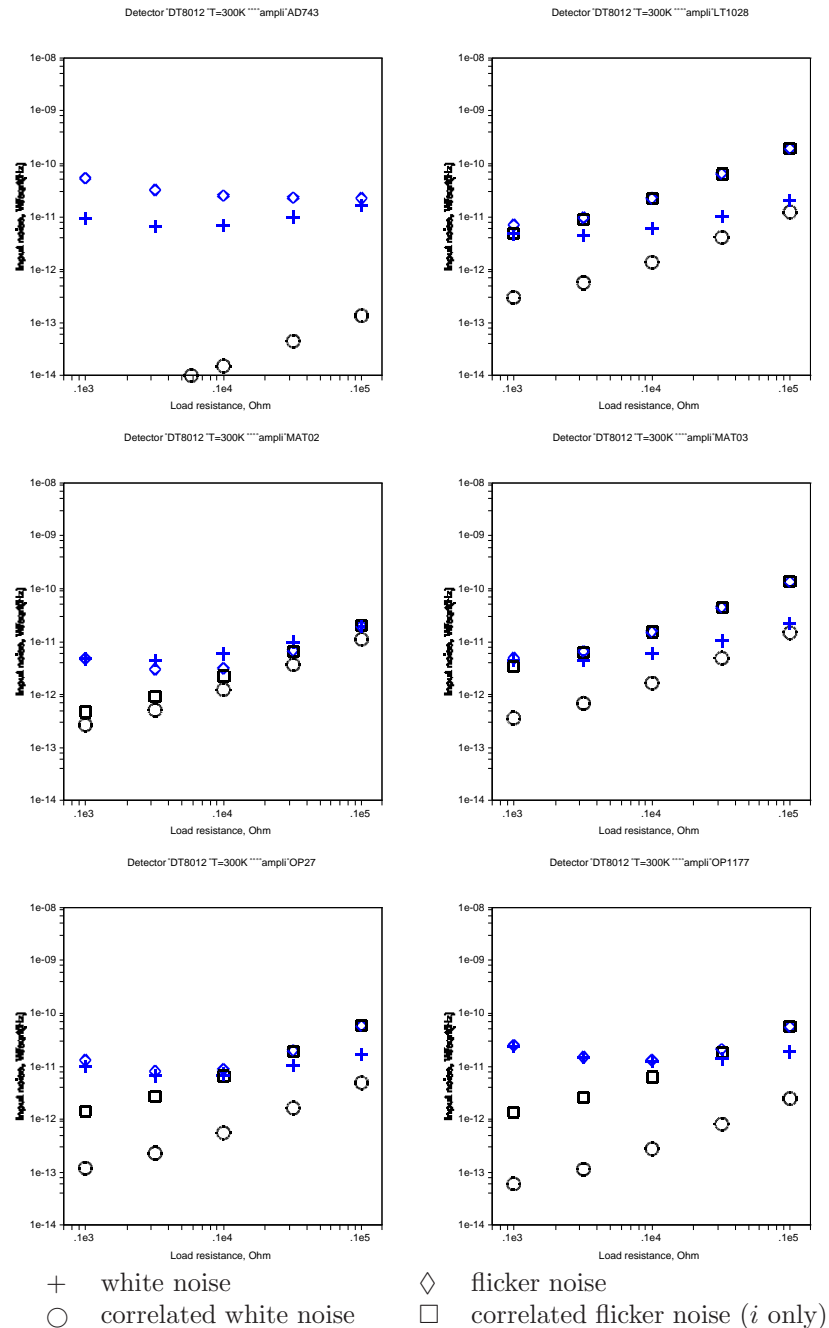


Figure 13: Expected noise of the DT8012 (Tunnel) followed an amplifier.

Table 7: Expected noise of a power detector followed by an amplifier. The grey box shows the best choice for the amplifier-detector pair.

Equivalent input noise							
detector and amplifier	noise type	load resistance					unit
		100	320	1000	3200	10000	
DZR124AA and AD743	white	99.2	39.5	22.8	19.6	24.5	10^{-12} $\frac{W}{\sqrt{Hz}}$
	flicker	541	186	80.8	44.8	33.3	
	correl. white	0.050	0.042	0.052	0.089	0.205	
	correl. flicker	—	—	—	—	—	
DZR124AA and MAT02	white	54.7	27.5	19.6	19.8	29.2	10^{-12} $\frac{W}{\sqrt{Hz}}$
	flicker	48.6	17.7	10.4	13.5	29.9	
	correl. white	4.06	3.45	4.24	7.28	16.7	
	correl. flicker	7.22	6.13	7.54	12.9	29.8	
DZR124AA and OP27	white	102	40.3	23.1	20.0	25.6	10^{-12} $\frac{W}{\sqrt{Hz}}$
	flicker	131	48.0	29.4	39.5	87.8	
	correl. white	1.80	1.53	1.88	3.23	7.44	
	correl. flicker	21.2	18.0	22.1	38.0	87.4	
DT8012 and AD743	white	9.86	6.77	7.00	10.0	16.2	10^{-12} $\frac{W}{\sqrt{Hz}}$
	flicker	53.7	32.0	24.8	22.8	22.1	
	correl. white	0.005	0.007	0.016	0.045	0.135	
	correl. flicker	—	—	—	—	—	
DT8012 and LT1028	white	5.44	4.72	6.06	10.2	20.1	10^{-12} $\frac{W}{\sqrt{Hz}}$
	flicker	8.78	10.9	23.3	66.0	197	
	correl. white	0.448	0.657	1.45	4.12	12.3	
	correl. flicker	7.17	10.5	23.2	66.0	197	
DT8012 and MAT02	white	5.43	4.72	6.02	10.1	19.3	10^{-12} $\frac{W}{\sqrt{Hz}}$
	flicker	4.83	3.03	3.20	6.90	19.8	
	correl. white	0.403	0.591	1.30	3.71	11.1	
	correl. flicker	0.717	1.05	2.32	6.60	19.7	
White and shot noise, plus white and flicker noise of the amplifier. The flicker noise of the power detector is not accounted for.							

Detector DT8012 (tunnel)

AD743 and 1 kΩ. Best design for a correlation-and-averaging system. Slightly lower white noise can be obtained at lower R , yet at expenses of larger m and of larger flicker noise.

LT1028 and 100 Ω. Simple nearly-optimum design for real-time (single channel) systems. This configuration, as compared to the best one (MAT02 with 320 Ω load) shows white noise 1.2 dB higher, and flicker noise 9 dB higher.

MAT02 and $320\ \Omega$. Lowest white and flicker noise in real-time measurements (single-channel).

MAT02 and $100\ \Omega$. Close to the lowest white and flicker noise in real-time measurements (single-channel). Fairly good for correlation at moderate averaging, up to $m = 360$ for white noise, and $m = 90$ for flicker.

Remark. Generally, tunnel detectors show higher gain than Schottky detectors. The fact that they exhibit lower noise is a consequence. On the other hand, the Schottky detectors are often preferred because of wider bandwidth, and because of higher tolerance to electrical stress and to experimental errors.

8 The measurement of the power detector noise

A detector alone can be measured only if a reference source is available whose AM noise is lower than the detector noise, and if the amplifier noise can be made negligible. These are unrealistic requirements.

It is useful to compare two detectors, as in Fig. 14 A. The trick is to measure a differential signal $g(P_b - P_a) \approx 0$, which is not affected by the power fluctuation of the source. The lock-in helps in making the output independent of the power fluctuations. Some residual PM noise has no effect on the detected voltage.

One problem with the scheme of Fig. 14 A is that the measured noise is the sum of the noise of the two detectors, for the result relies upon the assumption that the two detectors are about equal. This is fixed with the correlation scheme of Fig. 14 B. The detector c is the device under test, while the two other detectors are used to cancel the fluctuations of the input power. Thus

$$g(P_c - P_a) \quad \text{and} \quad g(P_c - P_b)$$

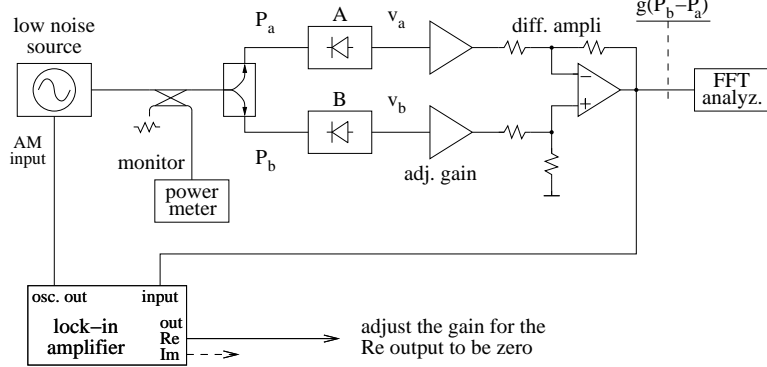
After rejecting the single-channel noise by correlation and averaging, there results the noise of the detector C.

Another problem with the schemes of Fig. 14 is that the noise of the amplifier is taken in. This is fixed by using two independent amplifiers at the output of the power detector, as in Fig. 15. In order to reject the current noise, these amplifiers must be of the JFET type. In the three detector scheme of Fig. 14 B, it is convenient to use BJT amplifiers in the reference branches (A and B), and a JFET amplifier in the branch C. The reason for this choice is the lower noise of the BJTs, which improves the measurement speed by reducing the minimum m needed for a given sensitivity.

9 AM noise in optical systems

Equation (1) also describes a quasi-perfect optical signal, under the same hypotheses 1–4 of page 4. The voltage $v(t)$ is replaced with the electric field. Yet,

A – Differential measurement



B – Three-detector correlation measurement

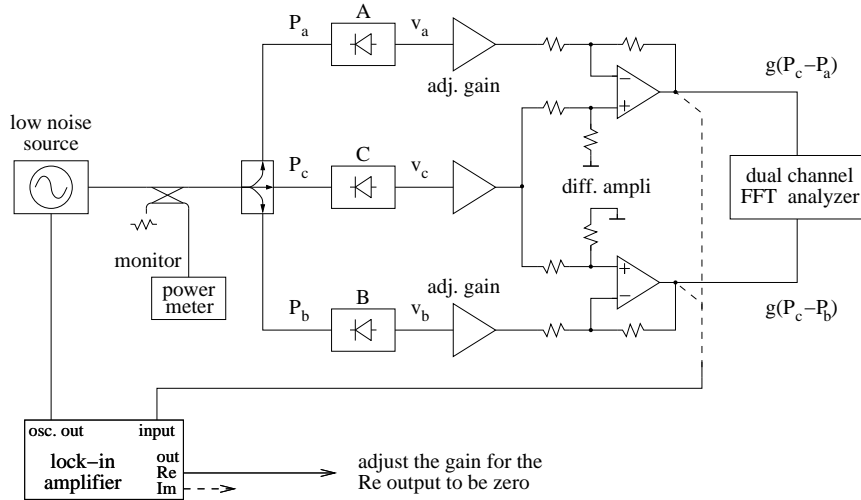


Figure 14: Measurement of the power detector noise.

the preferred physical quantity used to describe the AM noise is the Relative Intensity Noise (RIN), defined as

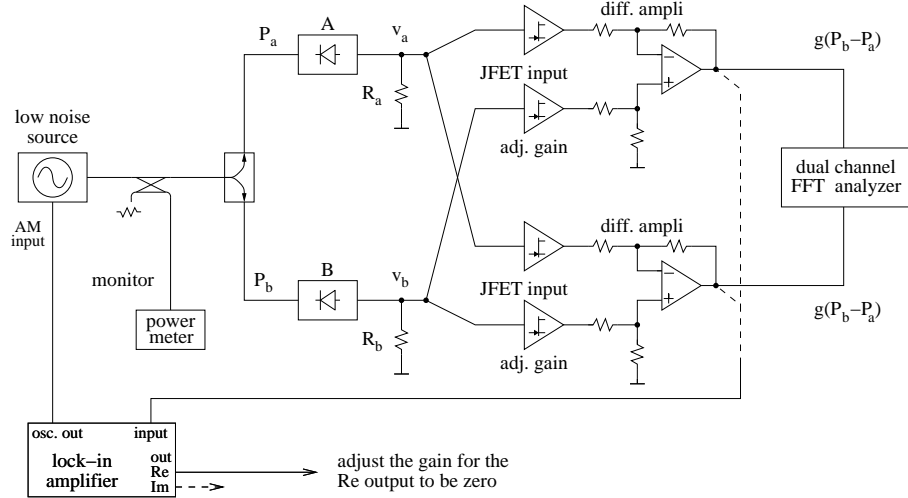
$$\text{RIN} = S_{\frac{\delta I}{I_0}}(f) , \quad (33)$$

that is, the power spectrum density of the normalized intensity fluctuation

$$\frac{(\delta I)(t)}{I_0} = \frac{I(t) - I_0}{I_0} . \quad (34)$$

The RIN includes both fluctuation of power and the fluctuation of the power cross-section distribution. If the cross-section distribution is constant in time,

A – Two-detector correlation measurement



B – Three-detector correlation measurement

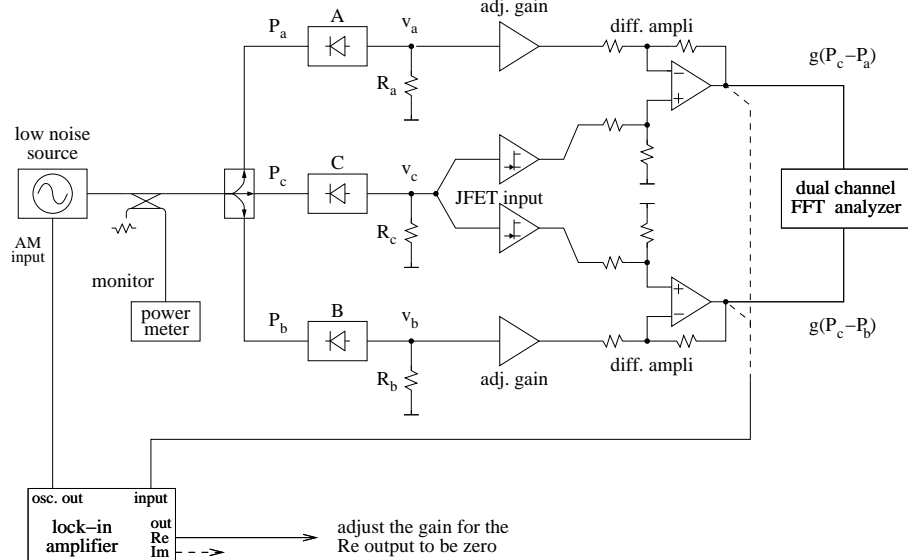


Figure 15: Improved scheme for the measurement of the power detector noise.

the optical intensity is proportional to power

$$\frac{\delta I}{I_0} = \frac{\delta P}{P_0} . \quad (35)$$

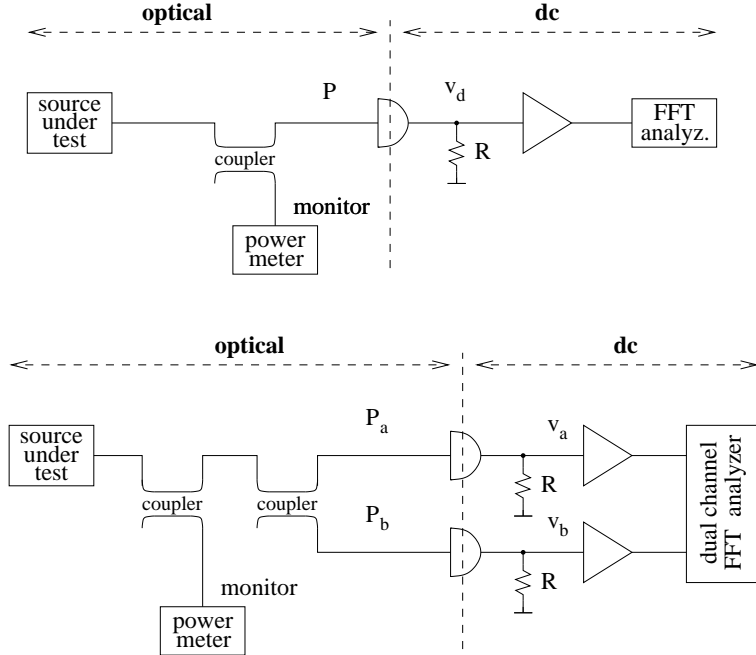


Figure 16: RIN measurement in optical-fiber systems. In a traditional system, beam splitters are used instead of the couplers.

In optical-fiber system, where the detector collects all the beam power, the term RIN is improperly used for the relative power fluctuation. Reference [SSL90] analyzes on the origin of RIN in semiconductor lasers, while References [Joi92, OS00] provide information on some topics of measurement.

In low-noise conditions, $|\delta I/I_0| \ll 1$, and assuming that the cross-section distribution is constant, the power fluctuations are related to the fractional amplitude noise α by

$$\frac{\delta I}{I_0} = \frac{\delta P}{P_0} = 2\alpha , \quad (36)$$

thus

$$\text{RIN}(f) = 4S_\alpha(f) . \quad (37)$$

Generally laser sources show a noise spectrum of the form

$$\text{RIN}(f) = h_0 + h_{-1}f^{-1} + h_{-2}f^{-2} , \quad (38)$$

in which the flicker noise can be hidden by the random walk. Additional fluctuations induced by the environment may be present.

Figure 16 shows two measurement schemes. The output signal of the photodetector is a current proportional to the photon flux. Accordingly, the gain parameter is the detector responsivity ϱ , defined by

$$i = \varrho P , \quad (39)$$

where

$$i = \frac{q\eta P}{h\nu} \quad (40)$$

is the photocurrent, thus

$$\varrho = \frac{q\eta}{h\nu} . \quad (41)$$

The schemes of Fig. 16 are similar to Fig. 1 (single-channel) and Fig. 2 (cross-spectrum). The dual-channel scheme is preferred because of the higher sensitivity, and because it makes possible to validate the measurement through the number of averaged spectra.

Noise is easily analyzed with the methods shown in Section 7. Yet in this case the virtual-ground amplifier is often preferred, which differs slightly from the examples shown in Section 7. A book [Gra96] is entirely devoted to the special case of the photodiode amplifier.

10 AM noise in microwave photonic systems

Microwave and rf photonics is being progressively recognized as an emerging domain of technology [Cha02, SJMN06]. It is therefore natural to investigate in noise in these systems.

The power⁵ $P_\lambda(t)$ of the optical signal is sinusoidally modulated in intensity at the microwave frequency ν_μ is

$$P_\lambda(t) = \bar{P}_\lambda (1 + m \cos 2\pi\nu_\mu t) , \quad (42)$$

where m is the modulation index⁶. Eq. (42) is similar to the traditional AM of radio broadcasting, but optical power is modulated instead of RF voltage. In the presence of a distorted (nonlinear) modulation, we take the fundamental microwave frequency ν_0 . The detector photocurrent is

$$i(t) = \frac{q\eta}{h\nu_\lambda} \bar{P}_\lambda (1 + m \cos 2\pi\nu_\mu t) , \quad (43)$$

where η the quantum efficiency of the photodetector. The oscillation term $m \cos 2\pi\nu_\mu t$ of Eq. (43) contributes to the microwave signal, the term “1” does not. The microwave power fed into the load resistance R_0 is $\bar{P}_\mu = R_0 \bar{i}^2$, hence

$$\bar{P}_\mu = \frac{1}{2} m^2 R_0 \left(\frac{q\eta}{h\nu_\lambda} \bar{P}_\lambda \right)^2 . \quad (44)$$

The discrete nature of photons leads to the shot noise of power spectral density $2qiR$ [W/Hz] at the detector output. By virtue of Eq. (43),

$$N_s = 2 \frac{q^2 \eta}{h\nu_\lambda} \bar{P}_\lambda R \quad (\text{shot noise}) . \quad (45)$$

⁵In this section we use the subscript λ for ‘light’ and μ for ‘microwave’.

⁶We use the symbol m for the modulation index, as in the general literature. There is no ambiguity because the number of averages (m) is not used in this section.

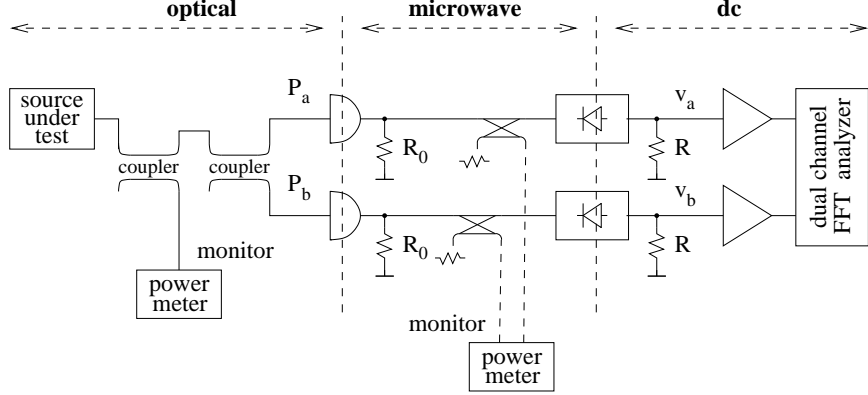


Figure 17: Measurement of the microwave AM noise of a modulated light beam.

In addition, there is the equivalent input noise of the amplifier loaded by R , whose power spectrum is

$$N_t = FkT \quad (\text{thermal noise and amplifier noise}), \quad (46)$$

where F is the noise figure of the amplifier, if any, at the output of the photodetector. The white noise $N_s + N_t$ turns into a noise floor

$$S_\alpha = \frac{N_s + N_t}{\bar{P}_\mu}. \quad (47)$$

Using (44), (45) and (46), the floor is

$$S_\alpha = \frac{2}{m^2} \left[2 \frac{h\nu_\lambda}{\eta} \frac{1}{\bar{P}_\lambda} + \frac{FkT}{R} \left(\frac{h\nu_\lambda}{q\eta} \right)^2 \left(\frac{1}{\bar{P}_\lambda} \right)^2 \right]. \quad (48)$$

Interestingly, the noise floor is proportional to $(\bar{P}_\lambda)^{-2}$ at low power, and to $(\bar{P}_\lambda)^{-1}$ above the threshold power

$$P_{\lambda,t} = \frac{1}{2} \frac{FkT}{R} \frac{h\nu_\lambda}{q^2\eta} \quad (49)$$

For example, taking $\nu_\lambda = 193.4$ THz (wavelength $\lambda = 1.55 \mu\text{m}$), $\eta = 0.6$, $F = 1$ (noise-free amplifier), and $m = 1$, we get a threshold power $P_{\lambda,t} = 335 \mu\text{W}$, which sets the noise floor at $5.1 \times 10^{-15} \text{ Hz}^{-1}$ (-143 dB/Hz).

Figure 17 shows the scheme of a correlation system for the measurement of the microwave AM noise. It may be necessary to add a microwave amplifier at the output of each photodetector. Eq. (48) holds for one arm of Fig. 17. As there are two independent arms, the noise power is multiplied by two.

Finally, it is to be pointed out that the results of this section concern only the white noise of the photodetector and of the microwave amplifier at the photodetector output. Experimental method and some data in the close-in microwave

flickering of the high-speed photodetectors is available in Reference [RSYM06]. The noise of the microwave power detector and of its amplifier is still to be added, according to Section 6.

11 Calibration

For small variations ΔP around a power P_0 , the detector gain is replaced by the differential gain

$$k_d = \frac{dv_d}{dP} . \quad (50)$$

which can be rewritten as

$$k_d = \frac{\Delta v_d}{\frac{\Delta P}{P_0} P_0} . \quad (51)$$

Equations (10)–(11), which are used to get $S_\alpha(f)$ from the spectrum $S_v(f)$ of the output voltage in single-channel measurements, rely upon the knowledge of the calibration factor $k_d P_0$. The separate knowledge of k_d and P_0 is not necessary because only the product $k_d P_0$ enters in Eq. (10)–(11). Therefore we can get $k_d P_0$ from

$$k_d P_0 = \frac{\Delta v_d}{\Delta P / P_0} . \quad (52)$$

This is a fortunate outcome for the following reasons

- A variable attenuator inserted in series to the oscillator under test sets a static $\delta P/P_0$ that is the same in all the circuit; this is a consequence of linearity. For reference,

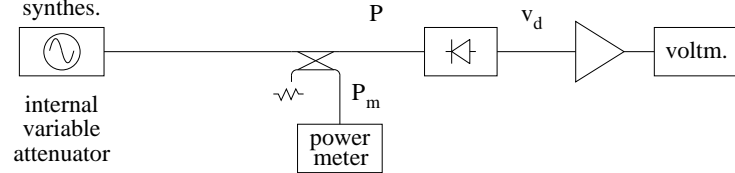
step, dB	$\Delta P/P_0$
0.1	2.33×10^{-2}
0.5	0.122
1	0.259

- A power ratio can be measured (or set) more accurately than an absolute power.

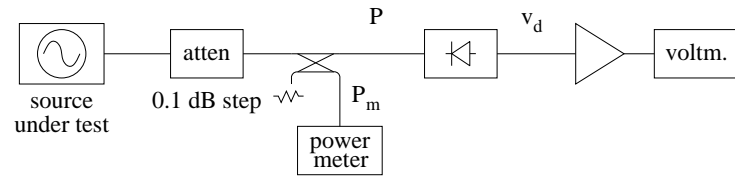
Some strategies can be followed (Fig. 18), depending on the available instrumentation. In all cases it is recommended to

- make sure that the power detector works in the quadratic region (see Fig. 5) by measuring the power at the detector input.
- exploit the differential accuracy of the instruments that measure ΔP and ΔV , instead of the absolute accuracy. Use the “relative” function if available, and do not change input range.

A – Synthesizer



B – By-step attenuator



C – Correlation system

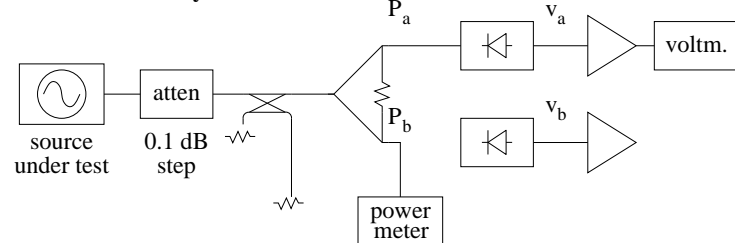
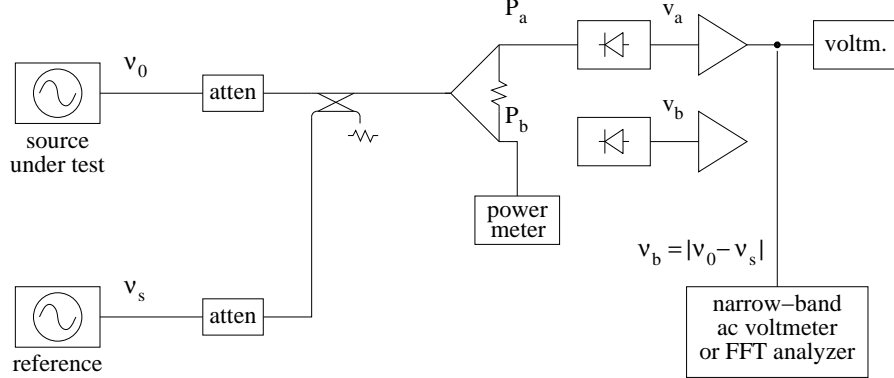


Figure 18: Calibration schemes.

- avoid plugging and unplugging connectors during the measurement. A directional coupler is needed not to disconnect the power detector for the measurement of ΔP .

In Fig. 18 A, the internal variable attenuator of a synthesizer is used to measure $k_d P_0$. $\Delta P/P_0$ can be measured with the power meter, or obtained from the calibration of the synthesizer internal attenuator. Some modern synthesizers have a precise attenuator that exhibit a resolution of 0.1 or 0.01 dB. In Fig. 18 B, a calibrated by-step attenuator is inserted between the source under test and the power detector. By-step attenuators can be accurate up to some 3–5 GHz. Beyond, one can use a multi-turn continuous attenuator and rely on the power meter. In the case of correlation measurements (Fig. 18 C), symmetry is exploited to measure k_a and k_b in a condition as close as possible to the final measurement of $S_\alpha(f)$. Of course, it holds that $\Delta P_a/P_a = \Delta P_b/P_b$.

B – AC calibration



B – Improved AC calibration

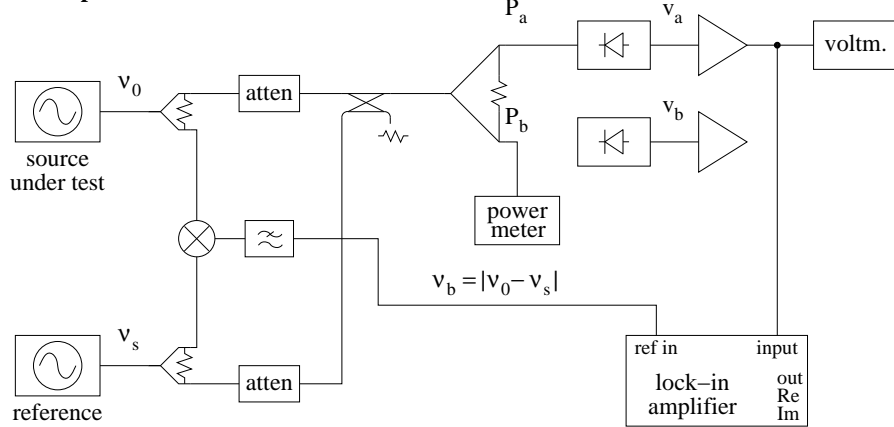


Figure 19: Alternate calibration schemes.

11.1 Alternate calibration method

Another method to calibrate the power detector makes use of two synthesizers in the frequency region of interest, so that the beat note falls in the audio frequencies (Fig. 19). This scheme is inspired to the two-tone method, chiefly used to measure the deviation of the detector from the ideal law $v_d = k_d P$ [RST⁺95, WCS04].

Using $P = \frac{v^2}{R}$, and denoting the carrier and the reference sideband with $v_0(t) = V_0 \cos(2\pi\nu_0 t)$ and $v_s(t) = V_s \cos(2\pi\nu_s t)$, respectively, the detected signal

is

$$v_d(t) = \frac{k_d}{R} \left\{ v_0(t) + v_s(t) \right\}^2 * h_{lp}(t) . \quad (53)$$

The low-pass function h_{lp} keeps the dc and the beat note at the frequency $\nu_b = \nu_s - \nu_0$, and eliminates the $\nu_s + \nu_0$ terms. Thus,

$$v_d(t) = \frac{k_d}{R} \left\{ \frac{1}{2} V_0^2 + \frac{1}{2} V_s^2 + 2 \frac{1}{2} V_0 V_s \cos [2\pi(\nu_s - \nu_0)t] \right\} , \quad (54)$$

which is split into the dc term

$$\bar{v}_d = k_d \frac{V_0^2 + V_s^2}{2R} \quad (55)$$

and the beat-note term

$$\tilde{v}_d(t) = 2 \frac{k_d}{R} \frac{V_0 V_s}{2} \cos [2\pi(\nu_s - \nu_0)t] , \quad (56)$$

hence

$$(V_d)_{\text{rms}} = k_d \sqrt{2P_0 P_s} . \quad (57)$$

The dc term [Eq. (55)] makes it possible to measure k_d from the contrast between \bar{v}_1 , observed with the carrier alone, and \bar{v}_2 , observed with both signals. Thus,

$$k_d = \frac{\bar{v}_2 - \bar{v}_1}{P_s} \quad (58)$$

Alternatively, the ac term [Eq. (57)] yields

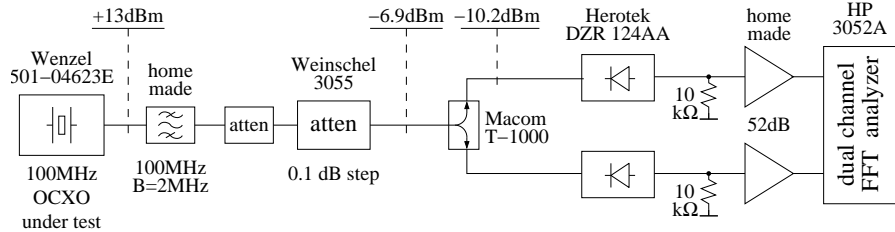
$$k_d = \frac{(V_d)_{\text{rms}}}{\sqrt{2P_0 P_s}} \quad (59)$$

The latter is appealing because the assessment of k_d relies only on ac measurements, which are free from offset and thermal drift. On the other hand, the two-tone measurement does not provide the straight measurement of the product $k_d P_0$.

12 Examples

Figure 20 show an example of AM noise measurement. The source under test is a 100 MHz quartz oscillator (Wenzel 501-04623E serial no. 3752-0214).

Calibration is done by changing the power $P_0 = -10.2$ dBm by ± 0.1 dB. There results $k_a = 1.28 \times 10^5$ V/W and $k_b = 1.34 \times 10^5$ V/W, including the 52 dB amplifier (321 V/W and 336 V/W without amplification). The system gain is therefore $4k_a k_b P_a P_b = 641$ V² (28.1 dBV²).



Wenzel 501-04623E (s/n 3572-0214)

$P_d = 9.5 \mu\text{W}$ (-10.2 dBm)
 $k_d = 1.31 \times 10^5 \text{ A}^{-1}$ with dc ampli
 $m = 638$ averaged spectra
 $1/\sqrt{2m} = 35.7$ (15.5 dB)
 $h_{-1} = 1.15 \times 10^{-12} \text{ Hz}^{-1}$ (-129.4 dB)
 $\sigma_\alpha = 4 \times 10^{-7}$

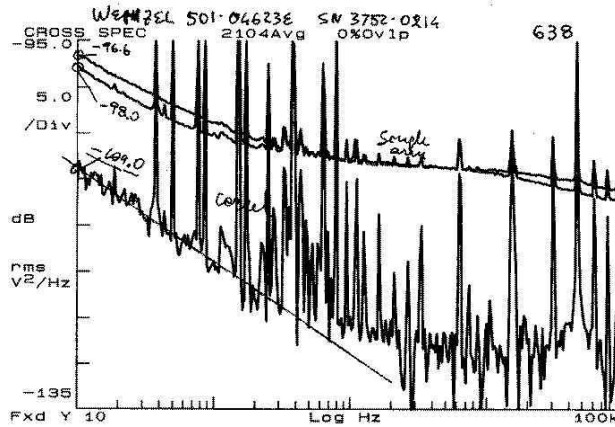


Figure 20: Example of AM noise measurement.

The cross spectrum of Fig. 20 is $S_{ba} = 1.26 \times 10^{-11} \text{ V}^2$ ($-109 \text{ dBV}^2/\text{Hz}$) at 10 Hz, of the flicker type. Averaging over $m = 638$ spectra, the single-channel noise is rejected by $\sqrt{2 \times 638} = 35.7$ (15.5 dB). The displayed flicker (-109 dB at 10 Hz) exceeds by only 3.8 dB the rejected single-channel noise. A correction of a factor 0.58 (-2.3 dB) is therefore necessary. The corrected flicker is $S_{ba} = 7.4 \times 10^{-11} \text{ V}^2$ ($-101.3 \text{ dBV}^2/\text{Hz}$) extrapolated at 1 Hz. The white noise can not be obtained from Fig. 20 because of the insufficient number of averaged spectra.

As a consequence of the low amplitude noise of the oscillator, it is possible to measure the noise of single channel, which includes detector and amplifier. Accounting for the gain (28.1 dBV²), the single-channel flicker noise of Fig. 20 at 1 Hz is $S_\alpha(1 \text{ Hz}) = 2.5 \times 10^{-12} \text{ Hz}^{-1}$ (-116.1 dB/Hz) for one channel, and

Table 8: AM noise of some sources.

source	h_{-1}	σ_α	notes
Anritsu MG3690A synthesizer (10 GHz)	2.5×10^{-11} −106.0 dB	5.9×10^{-6}	Fig. 21 A
Marconi synthesizer (5 GHz)	1.1×10^{-12} −119.6 dB	1.2×10^{-6}	
Macom PLX 32-18 0.1 → 9.9 GHz multiplier	1.0×10^{-12} −120.0 dB	1.2×10^{-6}	Fig. 22 A
Omega DRV9R192-105F 9.2 GHz DRO	8.1×10^{-11} −100.9 dB	1.1×10^{-6}	Fig. 21 B bump and junks
Narda DBP-0812N733 amplifier (9.9 GHz)	2.9×10^{-11} −105.4 dB	6.3×10^{-6}	Fig. 22 A/B
HP 8662A no. 1 synthesizer (100 MHz)	6.8×10^{-13} −121.7 dB	9.7×10^{-7}	Fig. 21 C junks
HP 8662A no. 2 synthesizer (100 MHz)	1.3×10^{-12} −118.8 dB	1.4×10^{-6}	Fig. 21 D junks
Fluke 6160B synthesizer	1.5×10^{-12} −118.3 dB	1.5×10^{-6}	Fig. 21 E junks
Racal Dana 9087B synthesizer (100 MHz)	8.4×10^{-12} −110.8 dB	3.4×10^{-6}	Fig. 21 F junks
Wenzel 500-02789D 100 MHz OCXO	4.7×10^{-12} −113.3 dB	2.6×10^{-6}	Fig. 20
Wenzel 501-04623E no. 1 100 MHz OCXO	2.0×10^{-13} −127.1 dB	5.2×10^{-7}	
Wenzel 501-04623E no. 2 100 MHz OCXO	1.3×10^{-13} −128.8 dB	4.3×10^{-7}	

$$S_\alpha(1 \text{ Hz}) = 3.4 \times 10^{-12} \text{ Hz}^{-1} (-114.7 \text{ dB/Hz}) \text{ for the other channel.}$$

The AM flickering of the oscillator is $S_\alpha(1 \text{ Hz}) = 1.15 \times 10^{-13} \text{ Hz}^{-1} (-129.4 \text{ dB/Hz})$, thus $h_{-1} = 1.14 \times 10^{-13}$. Using the conversion formula of Tab. 2 for flicker noise, the Allan variance is $\sigma_\alpha^2 = 1.6 \times 10^{-13}$, which indicates an amplitude stability $\sigma_\alpha = 4 \times 10^{-7}$, independent of the measurement time τ .

Table 8 shows some examples of AM noise measurement. The measured spectra are in Fig. 20, 21, and 22

All the experiments of Tab. 8 and Fig. 20, 21, and 22 were done before thinking seriously about the design of the front-end amplifier (Section 7), and before measuring the detector gain as a function of the load resistance (Table 5, and Figures 6–7). The available low-noise amplifiers, designed for other purposes, turned out to be a bad choice, far from being optimized for this application.

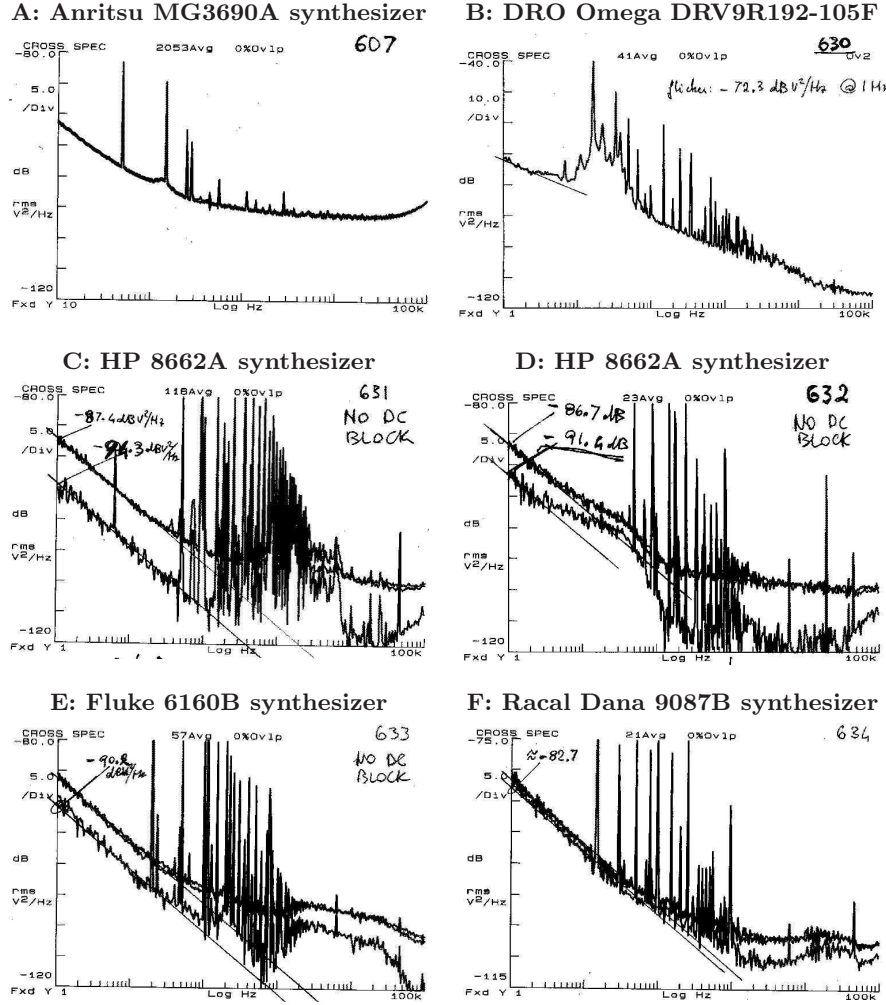


Figure 21: Examples of AM noise measurement.

Nonetheless, in all cases the observed cross spectrum is higher than the limit set by the average of two independent single-channel spectra. In addition, the limit set by channel isolation is significantly lower than the observed cross spectrum. These two facts indicate that the measured cross-spectrum is the true AM noise of the source. Thus Table 8 is an accurate database for a few specific cases. Of course, Table 8 also provides the order of magnitude for the AM noise of other synthesizers and oscillators employing similar technology. On the other hand, the data of Table 8 do not provide information on the detector noise.

The amplifier used in almost all the experiments is the “super-low-noise amplifier” proposed in the data sheet of the MAT03 [Pmi, Fig. 3], which is matched PNP transistor pair. For reference, the NPN version of this amplifier

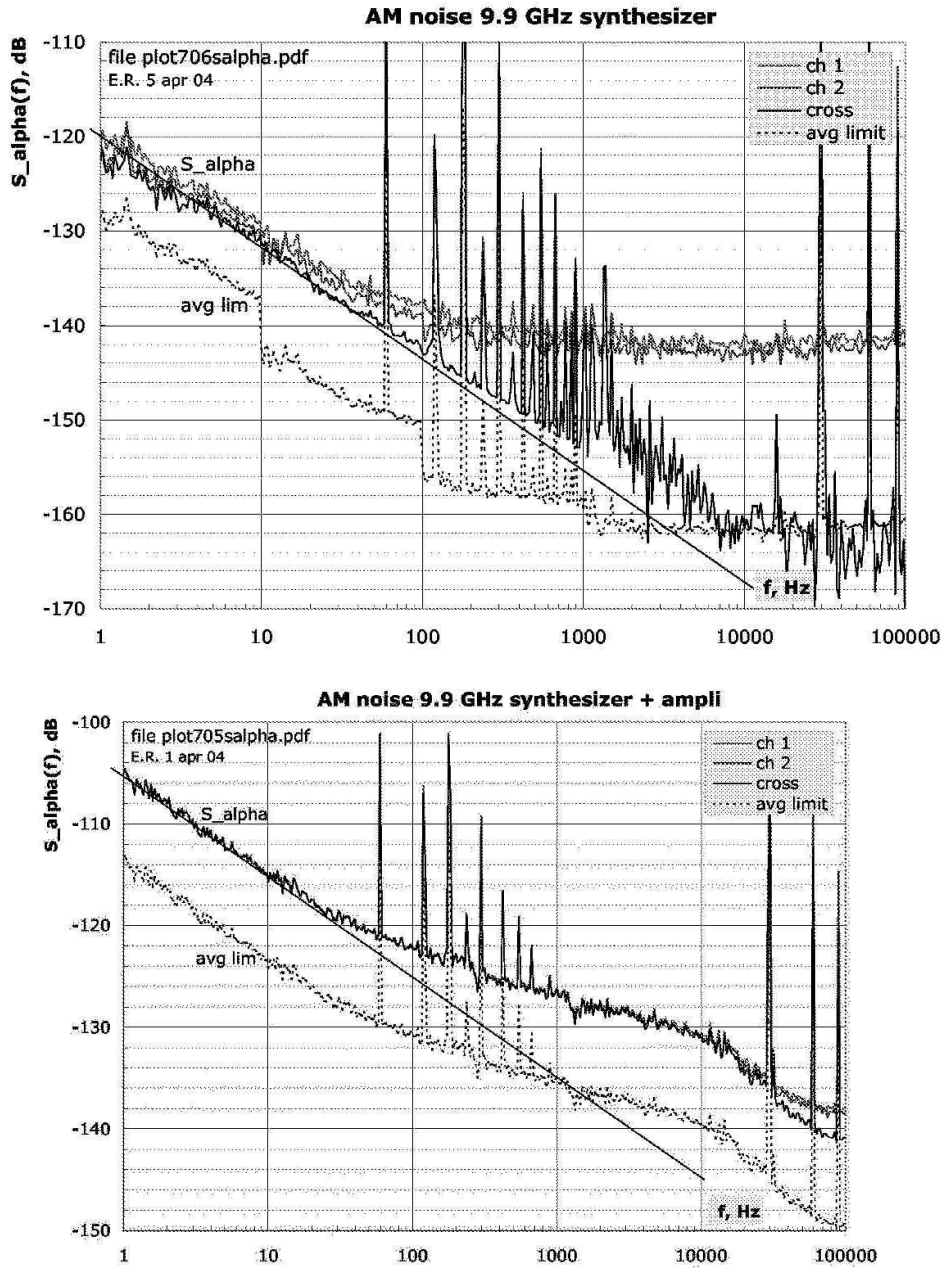


Figure 22: Examples of AM noise measurement.

is discussed in [Fra97]. The input differential stage of this amplifier consists of three differential pairs connected in parallel, so that the voltage noise is the

noise of a pair divided by $\sqrt{3}$. Yet the current noise is multiplied by $\sqrt{3}$. As a consequence, the amplifier is noise-matched to an impedance of some $200\ \Omega$ for flicker noise, and to some $30\ \Omega$ for white noise, which is too low for our purposes. The second version of the MAT03 amplifier, designed after the described experiments, was optimized for the lowest flicker when connected to a $50\ \Omega$ source [RLV04]. This amplifier, now routinely employed for the measurement of phase noise, makes use *one* MAT03 instead of three. In two cases (Fig. 22) a different amplifier was used, based on the OP37 operational amplifier loaded to an input resistance of some $1\ k\Omega$. Interestingly, in the operating conditions of AM noise measurements, the OP37 outperforms the more sophisticated MAT03.

13 Final remarks

True quadratic detection vs. peak detection. Beyond a threshold power, a power detector leaves the quadratic operations and works as a peak detector. The peak detection is the same operation mode of the old good detectors for AM broadcasting (which is actually an *envelope* modulation). This operation mode exhibits higher gain, hence it could be advantageous for the measurement of low-noise signals. The answer may depend on the diode type, Schottky or tunnel. The strong recommendation to use the diode in the quadratic region might be wrong.

Trans-resistance amplifiers. In principle, the power detector can be used as a power-to-current converter (instead of as a power-to-voltage) converter, and connected to a trans-resistance amplifier. The advantage is that the resistor at the detector output, which is a relevant source of noise in voltage-mode measurements, is not present. This choice, suggested in [Bur63], is never found in the technical literature accompanying the detectors.

Cryogenic environment. In principle, the tunnel diode should work at cryogenic temperatures. Yet, the laboratory could be much less smooth than the theory.

References

- [Agi03] Agilent Technologies, Inc., Paloalto, CA, *Fundamentals of RF and microwave power measurements, Part 1–4*, 2003. 4
- [Bur63] C. A. Burrus, *Backward diodes for low-level millimeter-wave detection*, IEEE Trans. Microw. Theory Tech. **11** (1963), no. 9, 357–362. 4, 13
- [Cha02] William S. C. Chang (ed.), *RF photonic technology in optical fiber links*, Cambridge, Cambridge, UK, 2002. 10

- [Eng61] Sverre T. Eng, *Low-noise properties of microwave backward diodes*, IRE Trans. Microw. Theory Tech. **9** (1961), no. 5, 419–425. 6
- [Fra97] Sergio Franco, *Design with operational amplifiers and analog integrated circuits*, 2nd ed., McGraw Hill, Singapore, 1997. 12
- [Gab67] William F. Gabriel, *Tunnel-diode low-level detection*, IEEE Trans. Microw. Theory Tech. **15** (1967), no. 10, 538–553. 4, 6
- [Gra96] Jerald G. Graeme, *Photodiode amplifiers*, McGraw Hill, Boston (MA), 1996. 9
- [Hal60] R. N. Hall, *Tunnel diodes*, IRE Trans. Electron Dev. (?) (1960), no. 9, 1–9. 4
- [Joi92] Irène Joindot, *Measurement of relative intensity noise (RIN) in semiconductor lasers*, J. Phys. III France **2** (1992), no. 9, 1591–1603. 9
- [NNW94] Lisa M. Nelson, Craig Nelson, and Fred L. Walls, *Relationship of AM to PM noise in selected RF oscillators*, IEEE Trans. Ultras. Ferroelec. and Freq. Contr. **41** (1994), no. 5, 680–684. 5, 8
- [OS00] Gregory E. Obarski and Jolene D. Splett, *Transfer standard for the spectral density of relative intensity noise of optical fiber sources near 1550 nm*, J. Opt. Soc. Am. B - Opt. Phys. **18** (2000), no. 6, 750–761. 9
- [Pmi] Analog Devices (formerly Precision Monolithics Inc.), *Specification of the MAT-03 low noise matched dual pnp transistor*, Also available as mat03.pdf on <http://www.analog.com/>. 12
- [RD56] H. Rothe and W. Dahlke, *Theory of noisy fourpoles*, Proc. IRE **44** (1956), 811–818. 7
- [RG02] Enrico Rubiola and Vincent Giordano, *Advanced interferometric phase and amplitude noise measurements*, Rev. Sci. Instrum. **73** (2002), no. 6, 2445–2457, Also on arxiv.org, document arXiv:physics/0503015v1. 1
- [RLV04] Enrico Rubiola and Franck Lardet-Vieudrin, *Low flicker-noise amplifier for 50Ω sources*, Rev. Sci. Instrum. **75** (2004), no. 5, 1323–1326, Free preprint available on arxiv.org, document arXiv:physics/0503012v1, March 2005. 7, 12
- [RST⁺95] Victor S. Reinhardt, Yi Chi Shih, Paul A. Toth, Samuel C. Reynolds, and Arnold L. Berman, *Methods for measuring the power linearity of microwave detectors for radiometric applications*, IEEE Trans. Microw. Theory Tech. **43** (1995), no. 4, 715–720. 11.1

- [RSYM06] Enrico Rubiola, Ertan Salik, Nan Yu, and Lute Maleki, *Flicker noise in high-speed p-i-n photodiodes*, IEEE Transact. MTT, special issue on Microwave Photonics (in press), February 2006, Free preprint available on arxiv.org, document arXiv:physics/0503022v1, March 2005. 10
- [SFF99] M. Sampietro, L. Fasoli, and G. Ferrari, *Spectrum analyzer with noise reduction by cross-correlation technique on two channels*, Rev. Sci. Instrum. **70** (1999), no. 5, 2520–2525. 7
- [SJMN06] Alwyn Seeds, Paul Juodawlkis, Javier Marti, and Tadao Nagatsuma (eds.), *IEEE Transactions on Microwave Theory and Techniques, special issue on microwave photonics*, IEEE, February 2006. 10
- [SSL90] C. B. Su, J. Schiafer, and R. B. Lauer, *Explanation of low-frequency relative intensity noise in semiconductor lasers*, Appl. Phys. Lett. **57** (1990), no. 9, 849–851. 9
- [WCS04] D. K. Walker, K. J. Coakley, and J. D. Splett, *Nonlinear modeling of tunnel diode detectors*, Proc. 2004 IEEE International Geoscience and Remote Sensing Symposium (IGARSS '04), vol. 6, 2004, pp. 3969–3972. 11.1